Effects of Mg substitution on the structural and magnetic properties of $Co_{0.5}Ni_{0.5-x}Mg_xFe_2O_4$ nanoparticle ferrites*

R M Rosnan†, Z Othaman, R Hussin, Ali A Ati, Alireza Samavati, Shadab Dabagh, and Samad Zare

Centre for Sustainable Nanomaterials, Ibnu Sina Institute for Scientific and Industrial Research, Universiti Teknologi Malaysia, 81310 *Skudai, Johor Bahru, Malaysia*

(Received 1 October 2015; revised manuscript received 16 December 2015; published online 25 February 2016)

In this study, nanocrystalline Co–Ni–Mg ferrite powders with composition $Co_{0.5}Ni_{0.5-x}Mg_xFe_2O_4$ are successfully synthesized by the co-precipitation method. A systematic investigation on the structural, morphological and magnetic properties of un-doped and Mg-doped Co–Ni ferrite nanoparticles is carried out. The prepared samples are characterized using x-ray diffraction (XRD) analysis, Fourier transform infrared spectroscopy (FTIR), field emission scanning electron microscopy (FESEM), and vibrating sample magnetometry (VSM). The XRD analyses of the synthesized samples confirm the formation of single-phase cubic spinel structures with crystallite sizes in a range of $\sim$ 32 nm to $\sim$ 36 nm. The lattice constant increases with increasing Mg content. FESEM images show that the synthesized samples are homogeneous with a uniformly distributed grain. The results of IR spectroscopy analysis indicate the formation of functional groups of spinel ferrite in the co-precipitation process. By increasing Mg^{2+} substitution, room temperature magnetic measurement shows that maximum magnetization and coercivity increase from $\sim$ 57.35 emu/g to $\sim$ 61.49 emu/g and $\sim$ 603.26 Oe to $\sim$ 684.11 Oe (1 Oe = 79.5775 A·m^{-1}), respectively. The higher values of magnetization M_s and M_r suggest that the optimum composition is $Co_{0.5}Ni_{0.4}Mg_{0.1}Fe_2O_4$ that can be applied to high-density recording media and microwave devices.

Keywords: co-precipitation; magnetic materials; spinel ferrite; magnetic properties

PACS: 75.47.Lx, 75.60.–d, 75.75.–c, 81.20.Fw **DOI:** 10.1088/1674-1056/25/4/047501

1. Introduction

The wide interest in ferrite nanoparticles is due to their unique and unusual chemical and physical properties with their high surface activities. A key factor for improving the properties of these particles due to their miniature size lies in enhancing the fraction of their surface atoms. It is useful in many applications such as recording media, microwave devices, pigments, high frequency cores, high-density magnetic information storage, absorbents, and sensors.[1–3]

Nanomaterials are mostly considered as materials in which the sizes of the particles or crystalline are below 100 nm in at least one or more dimensions. On a nano scale, a huge fraction of the atoms exist at (or close to) the surfaces of particles, which causes the unique characteristics of materials. Nanomaterials each have a large surface-to-volume ratio thus often exhibit amazing properties that differ from bulk ones. This type of structure belongs to a large class of compound that has a spinel type of structure. The structural and magnetic properties of nanocrystalline ferrites are affected by a variety of factors including processing conditions, sintering temperature, precursor atmosphere, chemical composition, cation distribution in the tetrahedral (A) and octahedral [B] sites, grain size, voids, surface layers, and doping.[4–7]

Spinel ferrites are made up of a regular combination of oxygen with the general formula of $(A)[B]_2O_4$. A crystal structure of spinel ferrite with the Fd-3m space group has 56 atoms. It contains 32 oxygen anions; 8 of 64 tetrahedral (A-site) and 16 of 32 octahedral interstitial sites (B-site) are filled by metal cations. The A-site cations are present in the interstices between 2 interpenetrating FCC lattices, while the B site cations reside in the interstices among 4 interpenetrating FCC lattices.[8,9] This special structure allows different metallic ions to be introduced to change its properties such as magnetic, electronic and other properties considerably.[10,11] A multitude of studies have focused on $NiFe_2O_4$ doped with other metal ions that provide improved magnetic properties for applications in the industry and medicine.[12,13]

Recently, the effect of Mg-doping on $NiCoZnFe_2O_4$ was studied and the coercive field was reported to decrease as a result of Mg doping. The maximum saturation magnetization (M_s) is present at $x = 0.05$.[14] Wang *et al.* studied the structural and magnetic properties of Mg-doped Co spinel ferrite and they found that M_s of $Co_{1-x}Mg_xFe_2O_4/SiO_2$ ferrite decreases with increasing Mg content.[15] It was reported that with the increase of MgO doping in $Ni_{1-x}A_xFe_2O_4$ nanoparticles, both M_s and H_c increase to 51.53 (emu/g) and 98.64 (Oe), respectively.[16]

There are several studies focusing on the effects of other co-substituted ferrites. The influences of magnetic ion substitution such as Ni^{2+},[17] Mn^{2+},[18] Gd^{3+},[19] and

*Project supported by the Ibnu Sina Institute for Scientific and Industrial Research, Physics Department of Universiti Teknologi Malaysia and the Ministry of Education Malaysia (Grant Nos. Q.J130000.2526.04H65).

†Corresponding author. E-mail: rizuanmr@gmail.com

© 2016 Chinese Physical Society and IOP Publishing Ltd

Cr^{3+}[20] on structural, magnetic, electric, and dielectric properties of $CoFe_2O_4$ have been investigated. Nevertheless, several researchers have reported on non-magnetic ions such as Al^{3+},[21] Y^{3+},[22] Zn^{2+},[23] Cu^{2+}[24] or Cd^{2+}[25] substituting $CoFe_2O_4$ and very few detailed studies of the Mg^{2+}. Magnesium ions with non-magnetic nature are known for achieving control over magnetic parameters in developing magnetic recording technology and they have a preference for strong B sites. Akther Hossain *et al.* observed that when the non-magnetic divalent cations such as Zn, Mg, are substituted for magnetic cations such as Ni, Co, Mn, the maximum magnetization (M_s) as well as the real part of the initial permeability ($m = i$) increases up to 50%.[26] $Ni_{1-x}Mg_xFe_2O_4$ was synthesized by John Berchmans *et al.* using citrate gel process. They suggested that Mg^{2+} ions cause appreciable changes in the structural and electrical properties of the ferrites.[27]

Motivated by these studies, we investigate the effects of magnesium concentration on the structural, morphological and magnetic properties of Mg substituted Co–Ni ferrites synthesized using the co-precipitation method sintered at 900 °C for 10 h. The improvement mechanism of the structural and magnetic properties is analyzed in detail.

2. Experiment

In our study, the chemical reagents for this experiment are nickel nitrate [$Ni(NO_3)_2.6H_2O$], magnesium nitrate [$Mg(NO_3)_2.6H_2O$], cobalt acetate [$Co(COO)_2.4H_2O$], and iron nitrate [$Fe(NO_3)_3.9H_2O$]. For sample preparation, initially the raw materials are prepared according to the prescribed composition ratios in the compound to be fabricated, and then are dissolved in de-ionized water. The aim of this step is to prepare the solution with the required concentration. A beaker and magnetic stirrer are used to mix these solutions constantly and then they are heated up to 80 °C. The NaOH solution (2.0 M) is added dropwise into the reaction mixture for precipitation and the pH is kept in a range of approximately 13. De-ionized water is used to wash the precipitates four times to remove the impurities, and then they are immediately dried at a temperature of 150 °C in an electric oven for water content removal purposes. These precipitates are then annealed in air at 900 °C for 10 h with a heating rate of 5 °C/min. Nanocrystalline $Co_{0.5}Ni_{0.5-x}Mg_xFe_2O_4$ powders with different crystallite sizes are prepared.

For confirmation of the spinel phase structure and the sample purity, the samples are characterized using an x-ray diffractometer (XRDM, D8 Advanced) with Cu K_α radiations $\lambda = 1.5406$ Å at 40 kV and 40 mA. The speed of scanning is set at ~ 2 °C/min with a resolution of 0.011 and 2θ scanning range from 20° to 70°. Field emission scan electron microscopy (FESEM) images are recorded using FESEM JEOL, JSM-6701F, operated at 5 kV. The elemental analysis is made by energy dispersive x-ray spectroscopy (EDX) attached with FESEM. Fourier transform infrared (FTIR) spectra are recorded using Perkin-Elmer 5DX FTIR after mixing 1 mg of the ferrite sample with 100 mg of potassium bromide (KBr). They are thoroughly mixed in mortar for 5 min until a fine mixture is obtained. Pellets of 10-mm diameter are then prepared from these samples. Hysteresis loops are measured using a vibrating sample magnetometer (VSM, LakeShore-7404) at room temperature with a maximum applied field of 12 kOe.

3. Results and discussion

The room temperature x-ray diffraction (XRD) patterns of samples are demonstrated in Fig. 1. The figure shows well-defined diffraction peaks and good crystallization in all samples. A single-phase cubic spinel structure can be indexed, for this pattern has no extra peaks such as α-Fe_2O_3. The diffraction pattern of the planes (220), (222), (311), (400), (422), (511), and (440) confirms the formation of a pure phase cubic spinel structure verified by the standard PDF cards (JCPDS NO. 01-088-0380). Referring to the inset in Fig. 1, the increasing of the Mg content in $Co_{0.5}Ni_{(0.5-x)}Mg_{(x)}Fe_2O_4$ leads to a continuous shift in 2θ towards a lower angle, which is corresponding to the increase of lattice parameters. The shift in the intense (311) peak toward a lower angle from 35.778° for $Co_{0.5}Ni_{0.5}Fe_2O_4$ to 35.539° for $Co_{0.5}Mg_{0.5}Fe_2O_4$ due to the change in the content of Mg is attributed to the variation in the lattice constant, which is presented in Table 1. By increasing the content of Mg, the intense peak becomes narrower, which indicates a higher degree of crystallinity and a larger particle size. The sizes of ferrite nanoparticles are estimated using the broadening of the (311) peak and Debye–Scherrer's equation[28] described as follows:

$$D_{(hkl)} = \frac{0.98\lambda}{\beta_{hkl}\cos\theta_{hkl}}, \tag{1}$$

where λ is the wave length of the x-ray radiation, k is a constant taken as 0.98, β is the full width at half maximum (FWHM) of line broadening, and θ is the angle of diffraction. The sizes of $Co_{0.5}Ni_{0.5-x}Mg_xFe_2O_4$ nanocrystallites are estimated to be in a range from ~ 32 nm to ~ 36 nm (Table 1). These nanoparticles are smaller than those reported by Raut *et al.* (45 nm–49 nm)[29] and Raju *et al.* (100 nm).[30] In addition, these nanocrystallines are small enough to be used in high-density recording media, thus obtaining the suitable signal-to-noise ratio.

Figure 2 indicates that the crystallite size increases from ~ 32.7 nm to ~ 35.8 nm with increasing Mg^{2+} ion substitution. The replacement of Ni^{2+} (0.69 Å) ions in octahedral B sites by Mg^{2+} (0.72 Å) causes the expansion of the unit cell, resulting in larger lattice constants.[31,32]

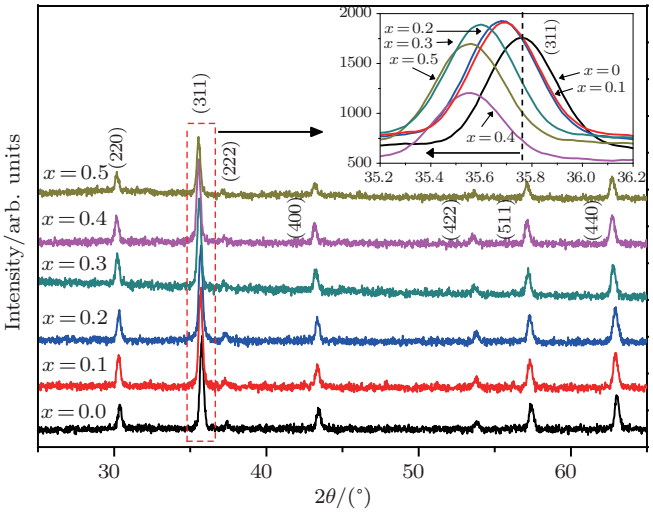


Fig. 1. (color online) X-ray diffraction patterns of $Co_{0.5}Ni_{0.5-x}Mg_xFe_2O_4$ ferrite nanoparticles.

Vegard's law is used to explain the relationship between Mg^{2+} substitution and lattice parameter.[33] The lattice constant (a), cell volume (V), and the x-ray density are calculated from the XRD spectra through using the following relations:

$$a = \sqrt{d^2(h^2+k^2+l^2)}, \tag{2}$$

$$V = a^3, \tag{3}$$

$$d_x = \frac{8M}{Na^3}, \tag{4}$$

where M is the molecular weight and N is the Avogadro number. The values of lattice parameter a (Å) calculated for the samples sintered at 900 °C are shown in Table 1.

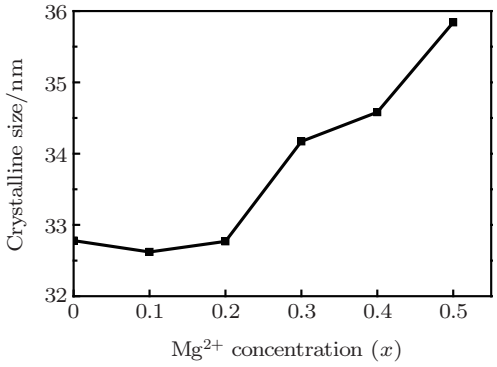


Fig. 2. Variation of crystalline size with Mg concentration.

Table 1. Characteristic parameters for each composition at room temperature.

$Co_{0.5}Ni_{0.5-x}Mg_xFe_2O_4$	ν_1/cm^{-1}	ν_2/cm^{-1}	Crystallite size D_m	d	a_{exp}/Å	V/Å^3	d_x/(g/cm^3)	d_B/(g/cm^3)	Porosity/%	S/(m^2/g)
$Co_{0.5}Ni_{0.5}Fe_2O_4$	594.95	398.55	32.8	2.511	8.328	577.55	5.393	4.223	21.70	43.44
$Co_{0.5}Ni_{0.4}Mg_{0.1}Fe_2O_4$	592.66	395.13	32.6	2.526	8.346	581.24	5.280	4.140	21.59	44.43
$Co_{0.5}Ni_{0.3}Mg_{0.2}Fe_2O_4$	591.52	390.56	32.7	2.515	8.343	580.66	5.207	4.056	22.10	45.14
$Co_{0.5}Ni_{0.2}Mg_{0.3}Fe_2O_4$	589.24	396.27	34.1	2.522	8.364	585.01	5.090	3.972	21.96	44.21
$Co_{0.5}Ni_{0.1}Mg_{0.4}Fe_2O_4$	586.95	397.41	34.5	2.525	8.374	587.28	4.993	3.889	22.11	44.62
$Co_{0.5}Mg_{0.5}Fe_2O_4$	584.67	399.55	35.8	2.525	8.375	587.32	4.915	3.806	22.56	43.99

It is observed from Fig. 3 that the x-ray density exhibits a decreasing trend from 5.393 g/cm^3 to 4.915 g/cm^3 with increasing Mg^{2+} substitution. The atomic weight of Mg is 25.31 amu, which is smaller than the atomic weight of Ni (58.69 amu), therefore, leads to the decrease of d_x with Mg^{2+} substitution increasing.

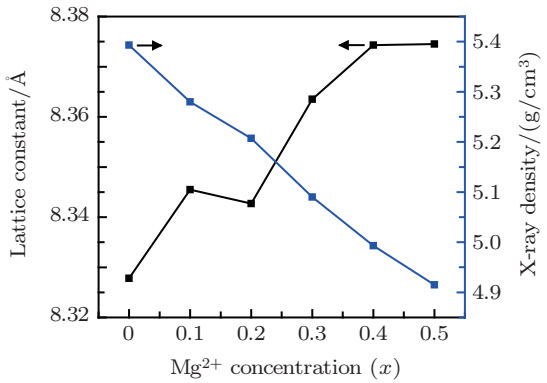


Fig. 3. (color online) Variations of lattice constant and x-ray density with Mg concentration.

The diameter of particle and the bulk density are used to estimate the specific surface area (S) from the following relation[34]

$$S = \frac{6000}{Dd_B}, \tag{5}$$

where D is the average crystallite size and d_B is the bulk density. The surface area (S) varies from 43.34 m^2/g to 43.99 m^2/g with Mg^{2+} content x increasing. The bulk density 'd_B' of the sample is determined by the hydrostatic method. The magnitude of the bulk density, d_B is smaller than that of the d_x due to the presence of pores created during the sintering. The curves of bulk density and porosity are opposite as expected with Mg^{2+} content. The percentage of porosity is calculated from the following relation:

$$P = \left(\frac{d_x - d_B}{d_x}\right) \times 100, \tag{6}$$

where d_x and d_B are the x-ray density and bulk density, respectively. It is observed that the porosity increases from 21.70 to 22.56 with increasing Mg^{2+} substitution as shown in Fig. 4. The increasing trend of porosity and lattice constant are inversely related to reducing the density of x-ray and bulk as expected.

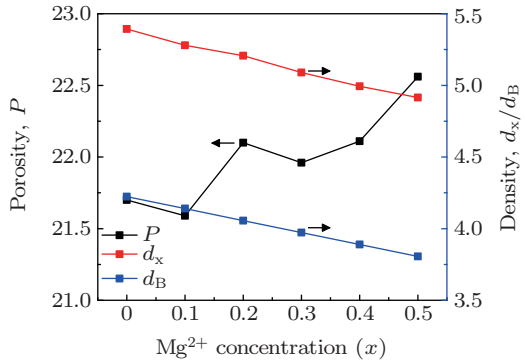


Fig. 4. (color online) Variations of x-ray density (d_x), bulk density (d_B), and porosity (P) with Mg^{2+} content x.

The field emission scan electron microscopy images of the co-precipitated $Co_{0.5}Ni_{0.5-x}Mg_xFe_2O_4$ ferrite samples sintered at 900 °C are shown in Fig. 5. As can be seen, the morphologies of these samples present regular shapes and dimensions. The average particle sizes of the samples for all the compositions, calculated using Image-J software are in a range of ∼ 35 nm to ∼ 80 nm. The surfaces of the ferrite samples appear to be rough and nanoparticles look like spheres in shape. The particles have no clear boundaries as they aggregate. The roughness of the surface may be due to the individual nanoparticles forming aggregates. The images indicate that the particles obtained by this synthesis method have homogenous morphology and uniform size, but partially agglomerate. The agglomeration is due to the slow growth of particles and also interactions existing between magnetic particles.

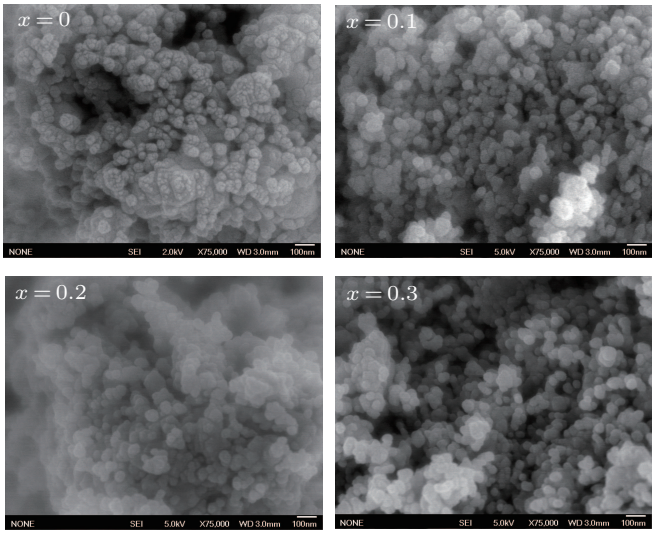


Fig. 5. FESEM images of $Co_{0.5}Ni_{0.5-x}Mg_xFe_2O_4$ nanoparticles sintered at 900 °C.

The EDX analyses (Figs. 6(a)–6(c)) of different compositions and various areas in the samples clearly reveal the existence of Fe, Co, Ni, Mg, and O elements. The occurrences of different atomic percentages of Ni and Mg confirm the different composition ratios of the samples which are listed in Table 2. The oxygen peak originates from the passivation of sample exposure to atmosphere during synthesis and characterization.

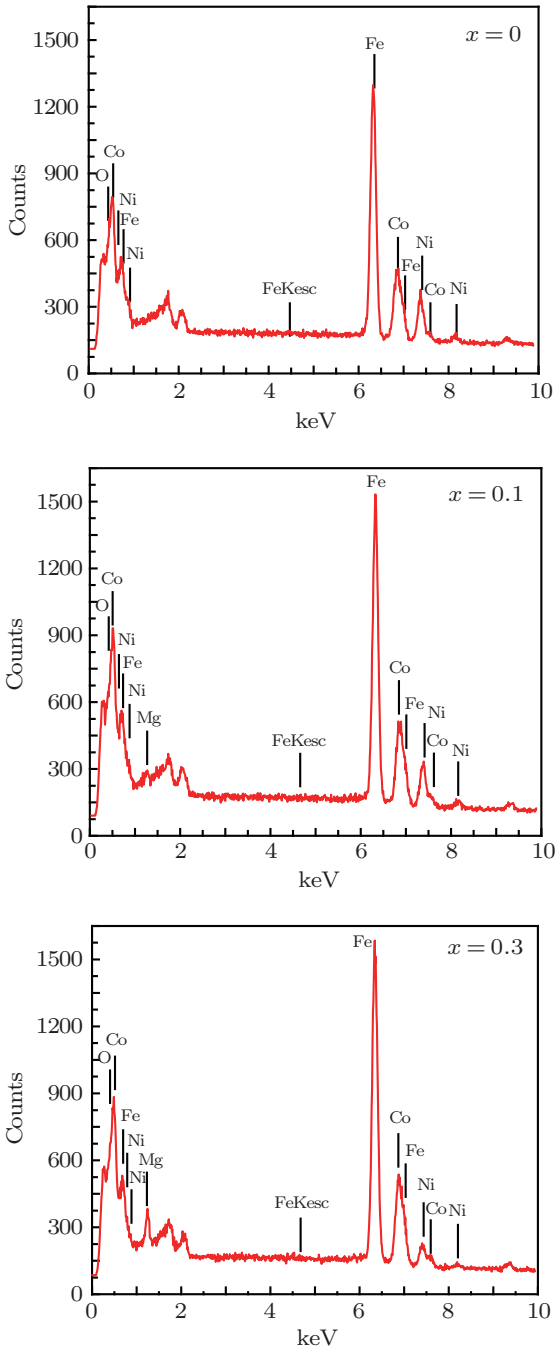


Fig. 6. (color online) EDX patterns of $Co_{0.5}Ni_{0.5-x}Mg_xFe_2O_4$ ferrites with different compositions of Mg substitution.

Table 2. Compositions of ferrite samples extracted from EDX analyses.

Composition	Fe	Co	Ni	Mg
$Co_{0.5}Ni_{0.5}Fe_2O_4$	1.92	0.58	0.50	–
$Co_{0.5}Ni_{0.4}Mg_{0.1}Fe_2O_4$	1.93	0.53	0.45	0.09
$Co_{0.5}Ni_{0.3}Mg_{0.2}Fe_2O_4$	1.97	0.51	0.34	0.18
$Co_{0.5}Ni_{0.2}Mg_{0.3}Fe_2O_4$	1.98	0.51	0.22	0.29

The infrared spectrum provides information about the positions of ions in the crystal and the crystal vibration modes, simplifying the probing different ordering phenomena. The formation of $Co_{0.5}Ni_{0.5-x}Mg_xFe_2O_4$ is studied by Fourier

transform infrared (FTIR) spectra at room temperature in a frequency range of 200 cm^{-1}–4000 cm^{-1} and the results are shown in Fig. 7. The bands appearing at the higher wave numbers ($\nu_1 = 585$ cm^{-1}–595 cm^{-1}) and at the lower wave numbers ($\nu_2 = 390$ cm^{-1}–400 cm^{-1}) are assigned to the tetrahedral complexes ($M_{tet} \leftrightarrow$O) and octahedral complexes ($M_{oct} \leftrightarrow$O), respectively.[35] The vibration mode of the tetrahedral cluster is normally higher than that of the octahedral cluster which could be attributed to the shorter and the longer bond length of each cluster. The observed absorption pattern reveals the formation of the spinel lattice, even a minimal intense band at around 550 cm^{-1} is sufficient for the spinel phase formation.[36] Hence, we assume that in the precipitation process aging the prepared mixture may lead to some degree of the spinel phase. The dried powders show characteristic bands at about 3400, and in ranges of 2850 cm^{-1}–3000 cm^{-1}, 1400 cm^{-1}–1700 cm^{-1}, and 1100 cm^{-1}–1300 cm^{-1}, which are ascribed to the O–H group symmetric vibration, the stretching of the C–H bands, carboxyl group (COO^-) and group symmetric vibration, respectively.[37] The combustion process causes all the hydroxyl, carboxyl and nitrate groups to appear with less intensity due to the generation of high temperature.

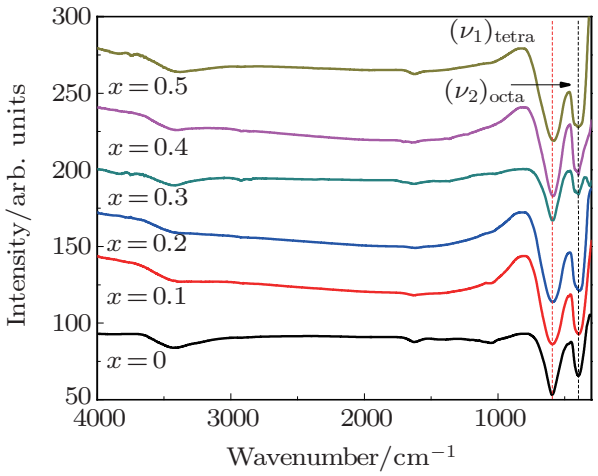


Fig. 7. (color online) Infrared spectra of $Co_{0.5}Ni_{0.5-x}Mg_xFe_2O_4$ system.

Hysteresis loops for $Co_{0.5}Ni_{0.5-x}Mg_xFe_2O_4$ $(0.0 \leq x \leq 0.5)$ ferrite samples are measured in order to obtain magnetic parameters as shown in Fig. 8. The values of maximum magnetizations for the as-prepared samples of $Co_{0.5}Ni_{0.5}Fe_2O_4$ and $Co_{0.5}Mg_{0.5}Fe_2O_4$ are found to be 57.35 emu/g and 49.25 emu/g, respectively. The cation distribution at the A- and B-sites, the super-exchange interaction and the non-collinear nature of B-site moments strongly affect the magnetizations in ferrites.

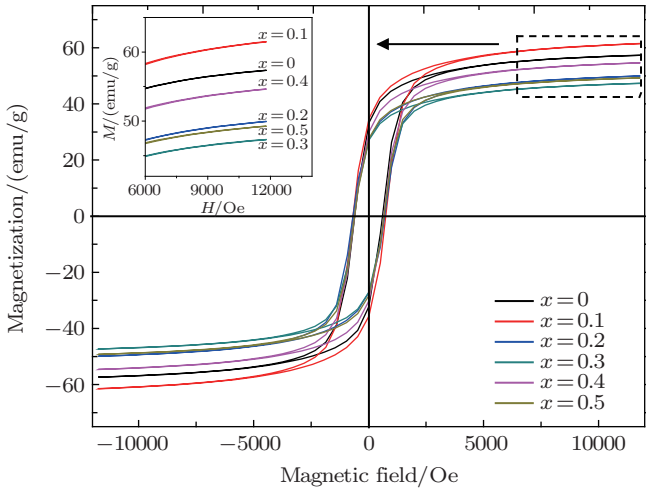


Fig. 8. (color online) Variations of magnetization (M) with applied field (H) of $Co_{0.5}Ni_{0.5-x}Mg_xFe_2O_4$ nanoparticles. The inset shows the partially magnified hysteresis curves at maximum applied field for a series of samples.

The magnetic parameters in Table 3 show that the value of M_s increases with increasing Mg substitution up to $x = 0.1$, thereafter it starts to decrease with increasing Mg substitution. This influence may be attributed to the weakening of super-exchange ion interaction at A site and B site due to non-magnetic Mg^{2+} ions.[38] The preference of Mg for both A- and B- sites can be attributed to the tendency of Mg^{2+} ions occupying A-sites, corresponding to Fe^{3+} ions migrating to the B-site. The replacement of the Fe^{3+} ion which has a higher magnetic moment than the Ni^{2+} ion results in the increase of the magnetic moment of the B sub-lattice.[39] Roy and Bera have reported a similar behavior of magnetization variation with Mg substitution.[40] It is also seen from Table 3 that the coercivity of the ferrite increases with Mg concentration increasing, the maximum value occurring at $x = 0.1$. The decrease of H_c is due to the increase of average grain size and the immoderate nonmagnetic ions entering into the lattices may result in the energy reduction of magnetocrystalline anisotropy.

Table 3. Room-temperature characteristic magnetic parameters for each composition.

$Co_{0.5}Ni_{0.5-x}Mg_xFe_2O_4$	H_c/Oe	M_r/(emu/g)	Maximum M/(emu/g)	M_r/M_s	Magnetic moment (bohr magneton)
$Co_{0.5}Ni_{0.5}Fe_2O_4$	603.26	32.43	57.35	0.57	2.41
$Co_{0.5}Ni_{0.4}Mg_{0.1}Fe_2O_4$	684.11	34.05	61.49	0.55	2.55
$Co_{0.5}Ni_{0.3}Mg_{0.2}Fe_2O_4$	681.12	27.09	49.93	0.54	2.04
$Co_{0.5}Ni_{0.2}Mg_{0.3}Fe_2O_4$	621.27	26.41	47.34	0.56	1.90
$Co_{0.5}Ni_{0.1}Mg_{0.4}Fe_2O_4$	608.17	29.13	54.62	0.53	2.16
$Co_{0.5}Mg_{0.5}Fe_2O_4$	606.17	26.83	49.25	0.54	1.92

The values of magnetic moment (η_B) can be calculated from the experimental hysteresis data by using the maximum magnetizations and the molecular weights of different samples.[41] The data reported in Table 3 obviously show that the magnetization and magnetic moment increase with doping level x till $x = 0.1$. Both M_s and η_B parameters start to decrease as the Mg content increases above $x = 0.1$, as expected since the Mg^{2+} ions with a zero magnetic moment tend to replace Ni^{2+} ions with a magnetic moment of 2.3 BM, at the octahedral sites. The variation of η_B with composition is explained on the basis of Neel's two-sublattice model of ferrimagnetisms.[42,43] In this model, the net magnetization $\eta_B(x)$ in BM is calculated from the following equation:

$$\eta_B(x) = MB(x) - MA(x), \tag{7}$$

where MA and MB are the sublattice magnetic moments at A and B sites, respectively. The higher Neel's magnetic moment $\eta_B(x)$ than η_B (Table 2) is attributed to the increase of the exchange interaction of the B-site on the expense of that of the A-site.[39] A similar behavior for Mg-substituted NiZn ferrites is reported by Bobade *et al.*[44] The achieved squareness ratio (M_r/M_s) of above 0.50 clearly indicates that the synthesized materials are in a single magnetic domain[45] and that they benefit the memory device application. The calculated squareness ratios for Mg-substituted Ni–Co ferrites are listed in Table 3. The sample with composition $Co_{0.5}Ni_{0.4}Mg_{0.1}Fe_2O_4$ is appropriate for use in a high-density recording medium where high maximum magnetization and coercivity above 600 Oe are desirable.[46]

4. Conclusions

The effects of Mg content on the structural, morphological, and magnetic properties of Ni-Mg doped Co-ferrite nanoparticles are examined. The XRD patterns for all samples confirm the single phase formation of these spinel ferrites. FESEM images demonstrate that the grains are homogenously distributed and become larger as the Mg content increases and enters into the spinel lattice. The grain size is calculated using Image-J software and found to be in a range from ~ 35 nm to ~ 80 nm, depending on the Mg content entering into the spinel lattice. The particle sizes are small enough to be used in high-density recording media for obtaining the suitable signal-to-noise ratio. The IR curves of sintered samples exhibit absorption bands at about 595 cm^{-1} and 400 cm^{-1}, which are due to the metal–oxygen stretching vibrations of tetrahedral and octahedral sites, respectively. The hysteresis loops show the improvement in the magnetic property especially in coercivity due to the substitution of Mg ions into the spinel lattice. The squareness ratio is above 0.5 which reveals a single magnetic domain of material. Owing to all these distinguished parameters, it is affirmed that the investigated materials have high potential applications in many areas such as high-frequency devices and core materials where low eddy current losses are required.

References

[1] Šepelák V, Baabe D, Mienert D, Schultze D, Krumeich F, Litterst F J and Becker K D 2003 *J. Magn. Magn. Mater.* **257** 377
[2] Ramana C V, Kolekar Y D, Kamala Bharathi K, Sinha B and Ghosh K 2013 *J. Appl. Phys.* **114** 183907
[3] Karanjkar M M, Tarwal N L, Vaigankar A S and Patil P S 2013 *Ceram. Int.* **39** 1757
[4] Tan M, Köseoğlu Y, Alan F and Şentürk E 2011 *J. Alloys Compd.* **509** 9399
[5] Patange S, Shirsath S E, Jangam Lohar G K, Jadhav S S and Jadhav K 2011 *J. Appl. Phys.* **109** 053909
[6] Islam M U, Abbas T, Niazi S B, Ahmad Z, Sabeen S and Chaudhry M A 2004 *Solid State Commun.* **130** 353
[7] He X M, Yan S M, Li Z W, Zhang X, Song X Y, Qiao W, Zhong W and Du Y W 2015 *Chin. Phys. B* **24** 127502
[8] Ati A A, Othaman Z and Samavati A 2013 *J. Mol. Struct.* **1052** 177
[9] Li L Z, Tu X Q, Wang R and Peng L 2015 *J. Magn. Magn. Mater.* **381** 328
[10] Joshi S, Kumar S M, Chhoker S, Srivastava G, Jewariya M and Singh V N 2014 *J. Mol. Struct.* **1076** 55
[11] Zhu X F and Chen L F 2011 *J. Magn. Magn. Mater.* **323** 3138
[12] Balaji S, Selvan R K, Berchmans L J, Angappan S, Subramanian K and Augustin C 2005 *Mater. Sci. Eng. B* **119** 119
[13] Rahimi M, Kameli P, Ranjbar M, Hajihashemi H and Salamati H 2013 *J. Mater. Sci.* **48** 2969
[14] Li L Z, Yu Z, Lan Z W, Sun K and Wu C J 2014 *Ceram. Int.* **40** 13917
[15] Wang L, Lu M, Liu Y, Li J, Liu M and Li H 2015 *Ceram. Int.* **41** 4176
[16] Deraz N M 2012 *Ceram. Int.* **38** 511
[17] Sontu U B, Yelasani V and Musugu V R R 2015 *J. Magn. Magn. Mater.* **374** 376
[18] Tsay C Y, Lin Y H and Jen S U 2015 *Ceram. Int.* **41** 5531
[19] Puli V S, Adireddy S and Ramana C V 2015 *J. Alloys Compd.* **644** 470
[20] Shang Z F, Qi W H, Ji D H, Xu J, Tang G D, Zhang X Y, Li Z Z and Lang L L 2014 *Chin. Phys. B* **23** 107503
[21] Aghav P S, Dhage V N, Mane M L, Shengule D R, Dorik R G and Jadhav K M 2011 *Physica B: Condens. Matter* **406** 4350
[22] Kumari S, Kumar V, Kumar P, Kar M and Kumar L 2015 *Adv. Powder Technol.* **26** 213
[23] Sundararajan M, Kennedy L J, Aruldoss U, Khadeer S, Vijaya J J and Dunn S 2015 *Mater. Sci. Semicond. Process.* **40** 1
[24] Sekhar B C, Rao G S N, Caltun O F, Lakshmi B D, Rao B P and Rao P S V S 2016 *J. Magn. Magn. Mater.* **398** 59
[25] Reddy C V, Byon C, Narendra Baskar B D, Srinivas G, Shim J and Prabhakar Vattikuti S V 2015 *Superlattices Microstruct.* **82** 165
[26] Akther Hossain A K M, Seki M, Kawai T and Tabata H 2004 *J. Appl. Phys.* **96** 1273
[27] John Berchmans L, Kalai Selvan R, Selva Kumar P and Augustin C 2004 *J. Magn. Magn. Mater.* **279** 103
[28] Mirzaee S, Farjami Shayesteh S and Mahdavifar S 2014 *Polymer* **55** 3713
[29] Raut A V, Barkule R S, Shengule D R, Jadhav K M 2014 *J. Magn. Magn. Mater.* **358–359** 87
[30] Raju K, Venkataiah G and Yoon D H 2014 *Ceram. Int.* **40** 9337
[31] Rezlescu N, Rezlescu E, Pasnicu C and Craus M 1994 *J. Phys: Condens. Mater.* **6** 5707

[32] Naeem M, Shah N A, Gul I H and Maqsood A 2009 *J. Alloys. Compd.* **487** 739
[33] Denton A R and Ashcroft N W 1991 *Phys. Rev. A* **43** 3161
[34] Reshak A H 2014 *J. Alloys Compd.* **589** 213
[35] Waldron R D 1955 *Phys. Rev.* **99** 1727
[36] Kumar V, Rana A, Kumar N and Pant R P 2011 *Int. J. Appl. Ceram. Technol.* **8** 120
[37] Priyadharsini P, Pradeep A, Rao P S and Chandrasekaran G 2009 *Mater. Chem. Phys.* **116** 207
[38] Pradeep A, Priyadharsini P and Chandrasekaran G 2008 *J. Magn. Magn. Mater.* **320** 2774
[39] Gabal M A 2009 *J. Magn. Magn. Mater.* **321** 3144
[40] Roy P K and Bera J 2006 *J. Magn. Magn. Mater.* **298** 38
[41] Gabal M A, El-Shishtawy R M and Al Angari Y M 2012 *J. Magn. Magn. Mater.* **324** 2258
[42] Nath S K, Rahman M M, Sikder S, Hakim M and Hoque S M 2013 *ARPN J. Sci. Tech.* **3** 106
[43] Yafet Y and Kittel C 1952 *Phys. Rev.* **87** 290
[44] Bobade D H, Rathod S M and Mane M L 2012 *Physica B: Condens. Matter* **407** 3700
[45] Panneer Muthuselvam I and Bhowmik R N 2010 *J. Magn. Magn. Mater.* **322** 767
[46] Iqbal M J, Ashiq M N, Hernandez-Gomez P and Munoz J M 2007 *Scripta Mater.* **57** 1093